

Flows in and around active region NOAA12118 observed with the GREGOR solar telescope and SDO/HMI

M. Verma,¹ C. Denker,¹ H. Balthasar,¹ C. Kuckein,¹ S.J. González Manrique,^{1,2} M. Sobotka,⁶ N. Bello González,³ S. Hoch,³, A. Diercke,^{1,2} P. Kummerow,^{1,2} T. Berkefeld,³ M. Collados,⁵ A. Feller,⁴ A. Hofmann,¹ F. Kneer,⁷ A. Lagg,⁴ J. Löhner-Böttcher,³ H. Nicklas,⁷ A. Pastor Yabar,^{5,10} R. Schlichenmaier,³ D. Schmidt,^{3,8} W. Schmidt,³ M. Schubert,³ M. Sigwarth,³ S.K. Solanki,^{4,9} D. Soltau,³ J. Staude,¹ K.G. Strassmeier,¹ R. Volkmer,³ O. von der Lühse,³ and T. Waldmann³

¹*Leibniz-Institut für Astrophysik Potsdam (AIP), Germany; mverma@aip.de*

²*Universität Potsdam, Institut für Physik und Astronomie, Germany*

³*Kiepenheuer-Institut für Sonnenphysik, Germany*

⁴*Max-Planck-Institut für Sonnensystemforschung, Germany*

⁵*Instituto de Astrofísica de Canarias, Spain*

⁶*Astronomical Institute, Academy of Sciences of the Czech Republic*

⁷*Institut für Astrophysik, Georg-August-Universität Göttingen, Germany*

⁸*National Solar Observatory, USA*

⁹*School of Space Research, Kyung Hee University, Korea*

¹⁰*Dept. Astrofísica, Universidad de La Laguna, Tenerife, Spain*

Abstract. Accurate measurements of magnetic and velocity fields in and around solar active regions are key to unlocking the mysteries of the formation and the decay of sunspots. High spatial resolution image and spectral sequences with a high cadence obtained with the GREGOR solar telescope give us an opportunity to scrutinize 3-D flow fields with local correlation tracking and imaging spectroscopy. We present GREGOR early science data acquired in 2014 July – August with the GREGOR Fabry-Pérot Interferometer and the Blue Imaging Channel. Time-series of blue continuum (λ 450.6 nm) images of the small active region NOAA 12118 were restored with the speckle masking technique to derive horizontal proper motions and to track the evolution of morphological changes. In addition, high-resolution observations are discussed in the context of synoptic data from the Solar Dynamics Observatory.

1. Introduction

With new instruments and improved observing facilities we can enhance our understanding of plasma motions surrounding sunspots and their interaction with magnetic fields. Current developments in the magneto-hydrodynamics (MHD) simulations (e.g.,

Rempel & Cheung 2014) provide the complete evolution of an active region from flux emergence to decay, allowing direct comparison with these high-resolution observations. In the growing phase, penumbra form rapidly around the sunspot (Leka & Skumanich 1998; Yang et al. 2003). The appearance of penumbrae is closely linked to inclined magnetic field lines and the onset of the Evershed flow. During the growth of the penumbra the umbral size seems to remain stable according to Schlichenmaier et al. (2010). It is common that the growth of sunspots is faster than the decay (e.g., Verma et al. 2012). The stable leading sunspots and irregular trailing spots decay with different rates (Martínez Pillet 2002). Many decay laws have been proposed ranging from a linear decay rate of Bumba (1963) to a parabolic decay law described by Petrovay & van Driel-Gesztelyi (1997).

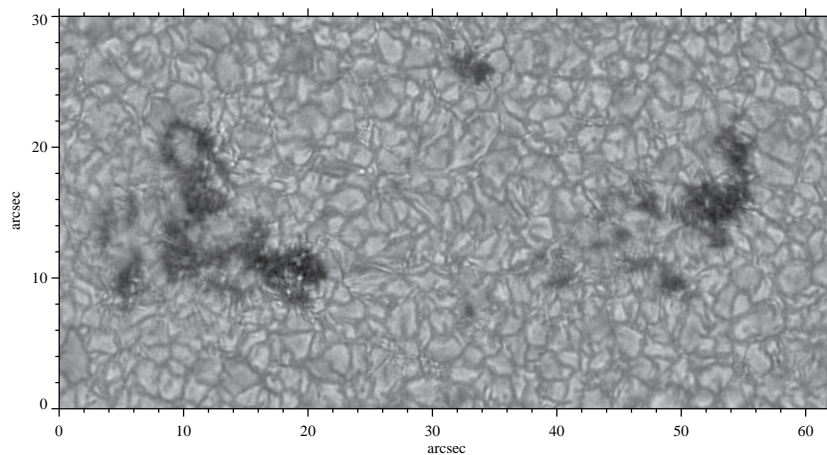


Figure 1. Bipolar active region NOAA 12118 observed in a blue continuum image of GREGOR/BIC on 2014 July 18. The image was rotated to match the orientation of the region in SDO images.

The flow structure around sunspots and active region plays significant role in both growth and decay processes. Magnetic flux from the sunspot is removed via the interaction of penumbral filaments and the surrounding granulation (Kubo et al. 2008). Unipolar moving magnetic features (e.g., Hagenaar & Shine 2005), which are usually observed around decaying sunspots (Harvey & Harvey 1973) and pores (Verma et al. 2012), are supposed to transport flux to surrounding supergranular cell boundaries. Hence, detailed knowledge of flow fields in and around solar magnetic features at various evolutionary stages is expected to provide insight into the growth and decay processes of sunspots. In this work based on GREGOR data, we present the horizontal proper motions around an active region, which is in its growth phase with continuous flux emergence.

2. Observations and data reduction

In July – August 2014 we had carried out a 50-day-long “early science” campaign at the 1.5-meter GREGOR solar telescope (Denker et al. 2012; Schmidt et al. 2012), which resulted in 30 days of observations with the Blue Imaging Channel (BIC) and the GREGOR Fabry-Pérot Interferometer (GFPI, Denker et al. 2010; Puschmann et al. 2012).

Here, we present time-series of blue continuum (λ 450.6 nm) images of the bipolar active region NOAA 12118 observed on 2014 July 18 starting at 07:56 UT. The four time-series of 30 min each were observed with 60 image sequences containing 80 images each with an exposure time of 4 ms. The images have a size of 2160×2672 pixels with an image scale of $0.035'' \text{ pixel}^{-1}$. The resulting field-of-view (FOV) of $75'' \times 93''$ fully contains the active region. The blue continuum images were reconstructed using the Kiepenheuer Institute Speckle Interferometry Package (KISIP, [Wöger et al. 2008](#); [Wöger & von der Lühe 2008](#)). Figure 1 shows an image from the blue continuum time-series. A region-of-interest (ROI) was extracted from the image and rotated to remove the image rotation introduced by the altitude-azimuth mount of the GREGOR telescope.

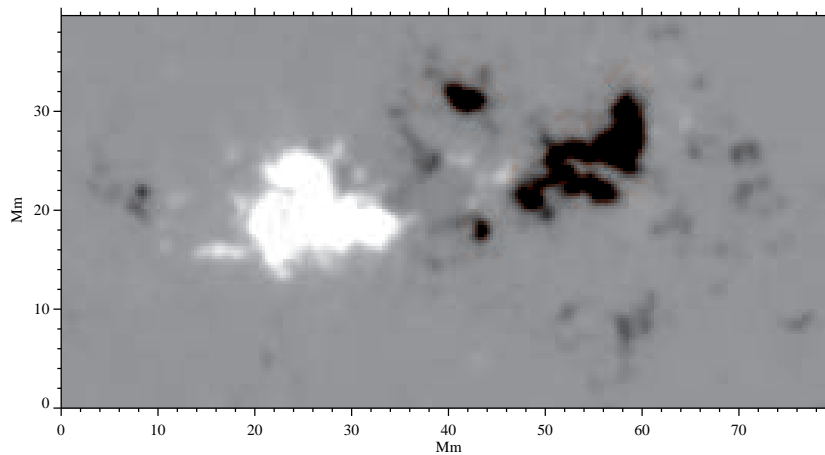


Figure 2. Active region NOAA 12118 as observed in a SDO/HMI LOS magnetogram. The magnetogram is displayed between ± 500 G.

We complemented GREGOR observations with the synoptic observations from the Solar Dynamics Observatory (SDO, [Scherrer et al. 2012](#)). SDO's Helioseismic and Magnetic Imager (HMI, [Schou et al. 2012](#); [Couvidat et al. 2012](#); [Wachter et al. 2012](#)) provided line-of-sight (LOS) magnetograms and continuum images covering the entire evolution of the active region, i.e., from its emergence to decay. The time-cadence of 45 s allowed us to use a time-series of LOS magnetograms for computing horizontal proper motions. Apart from basic calibration steps, magnetograms were corrected for geometrical foreshortening, after which a pixel represented 360 km on the solar surface. Figure 2 shows one of the magnetograms. The $40 \text{ Mm} \times 80 \text{ Mm}$ ROI was extracted from the full-disk magnetogram.

Active region NOAA 12118 appeared on the solar disk on 2014 July 17 around 15:00 UT. By the time of the GREGOR observations the region was approaching its maximum growth. However, the central part of the region was still a site for continuous flux emergence. The region was bipolar and categorized as an $\alpha\beta$ -group. The negative-polarity leading and positive-polarity trailing parts were both conglomerations of pores, which never developed penumbrae. The region started to decay on 2014 July 19. Atypically, the leading pore decayed first ([Bumba 1963](#)), and the region had significantly decayed by 2014 July 22.

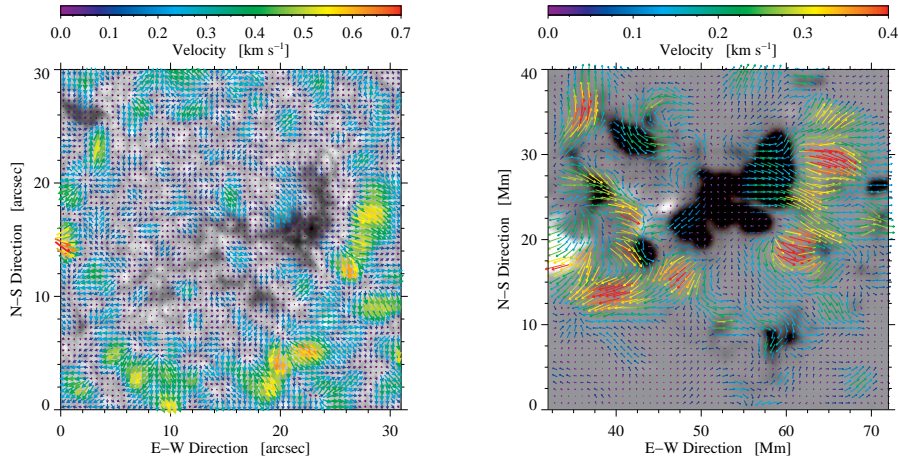


Figure 3. Detailed view of horizontal proper motions around the leading part of the active region computed using LCT (*left*) and DAVE (*right*). The coordinates refer to Figs. 1 and 2, respectively. In these images one arcsec corresponds to 0.78 Mm. The color figure can be found in the electronic version.

Horizontal proper motions using GREGOR continuum images were computed with the Local Correlation Tracking (LCT) code of [Verma & Denker \(2011\)](#). The code was adapted for high-resolution data. Images were aligned and the signature of five-minute oscillations was removed. Cross-correlations were computed over 48×48 -pixel image tiles with a Gaussian kernel having a FWHM = 1200 km, corresponding to the typical size of a granule. The time cadence was $\Delta t = 60$ s, and the flow maps were averaged over $\Delta T = 30$ min. Corresponding to GREGOR data we chose a 2-hour time-series of LOS magnetograms starting at 08:00 UT applying the Differential Affine Velocity Estimator (DAVE, [Schuck 2005, 2006](#)) to calculate the horizontal plasma velocities. We computed horizontal proper motions for all four time-series. However, considering the scope of this conference contribution we present preliminary results only for the second time-series, i.e., the 30-minute time-series starting 08:36 UT.

3. Results

To infer the proper motions in continuum images and magnetograms we used LCT and DAVE, respectively. These methods were applied to the full FOV. However, here we focus only on the leading pore of the active region (Fig. 3).

The observed active region was bipolar, with leading negative polarity. In the DAVE map (right-panel Fig. 3) there are strong outward motions along the border of the dominant pore. Inside the pores the horizontal velocities are lower and uniform. However, at coordinates (45 Mm, 22.5 Mm) in a region with mixed polarity the proper motion is multidirectional. At coordinates (47.5 Mm, 35 Mm) weak swirling motion is visible. The maximum DAVE velocity in the ROI reached up to 0.4 km s^{-1} .

The LCT map provides horizontal proper motions by tracking on photospheric features in continuum images. In the 30-minute averaged map of $30'' \times 30''$, we see high velocities in the surroundings of the pore giving an impression of moat flow. However, as already mentioned, none of the pores in the active region developed a penumbra, i.e.,

no Evershed flow can develop. In addition, many small scale diverging centers are visible, e.g., at coordinates ($2''$, $20''$) and ($14''$, $29''$). The LCT method tracks photospheric contrast features (granules, penumbral filaments, umbral dots, etc.) and does not per se rely on the presence of magnetic fields as in the case of DAVE. The maximum velocities achieved in the LCT map reach up to 0.7 km s^{-1} . Already visual inspection clearly reveals differences in velocities computed by DAVE and LCT. This discrepancy points to differences in the underlying physics used in both methods, but also the disparate spatial resolution has to be considered.

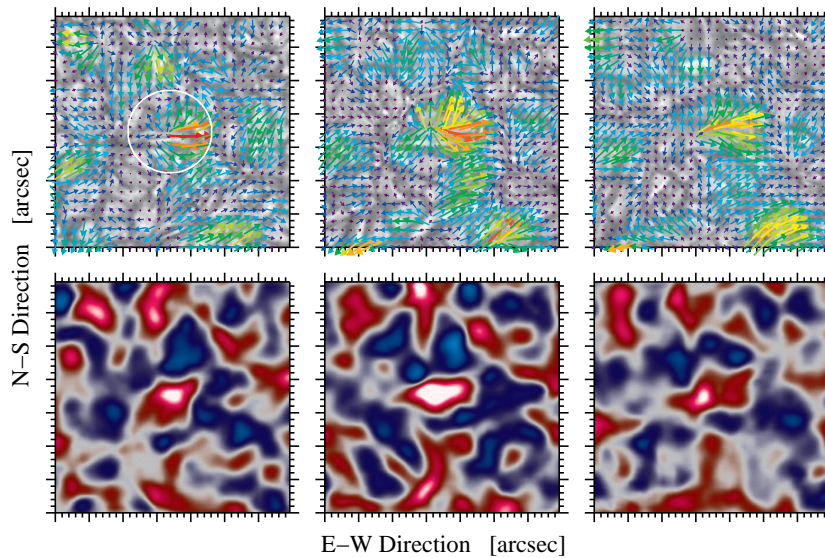


Figure 4. LCT velocities (*top*) and divergence (*bottom*) for one of the rapidly expanding granules marked by white circle over the period of 30 minutes. The FOV is $14'' \times 14''$. The rainbow-colored averaged LCT vectors are superposed on the 10-minute average continuum images of GREGOR, which capture the evolution of the rapidly expanding granule. Red colors represents divergence and blue corresponds to convergence. Divergence maps are scaled between $\pm 5 \times 10^{-2} \text{ s}^{-1}$. The color figure can be found in the electronic version.

The high spatial and temporal resolution of the GREGOR data allows us to follow horizontal proper motions of small-scale features such as *rapidly expanding granules*. In this active region, we see many granules which are larger and more elongated than normal granules. These rapidly expanding granules could be the signature of continuous flux emergence. One example of these expanding granules is shown in Fig. 4. We show an ROI of $14'' \times 14''$ centered on the granule. The horizontal flow maps are averaged over 10 min, and the background is the corresponding averaged blue continuum image. The center of the granule has a positive divergence from the start (as seen in the first panel of Fig. 4), which becomes highest in the next 10 minutes, while in the last 10 minutes it decreases. The LCT velocity vectors traced the full areal extent of the rapidly expanding granules.

4. Conclusion

The GREGOR high-resolution images and SDO LOS magnetograms furnished information about the evolution of horizontal flow fields around NOAA 12118. In the LCT and DAVE flow maps outward flows along the border of the leading pore were present. In addition, LCT captured the diverging proper motions of rapidly expanding granules. The presence of these granules in the region can be related to continuous flux emergence. In the future, the combination of spectropolarimetric observations of the GFPI and the GREGOR Infrared Spectrograph (GRIS, [Collados et al. 2012](#)) along with high-resolution imaging will provide the opportunity to follow changes in flows as well as magnetic fields. The multi-wavelength and multi-instrument setup is necessary to understand the complex process of spot formation and decay.

Acknowledgments. The 1.5-meter GREGOR solar telescope was build by a German consortium under the leadership of the Kiepenheuer-Institut für Sonnenphysik in Freiburg with the Leibniz-Institut für Astrophysik Potsdam, the Institut für Astrophysik Göttingen, and the Max-Planck-Institut für Sonnensystemforschung in Göttingen as partners, and with contributions by the Instituto de Astrofísica de Canarias and the Astronomical Institute of the Academy of Sciences of the Czech Republic. SDO HMI and AIA data are provided by the Joint Science Operations Center – Science Data Processing. MS is supported by the Czech Science Foundation under the grant 14-0338S. CD have been supported by grant DE 787/3-1 of the German Science Foundation (DFG). This study is supported by the European Commission’s FP7 Capacities Programme under the Grant Agreement number 312495.

References

- Bumba, V. 1963, *Bull. Astron. Inst. Czech.*, 14, 91
- Collados, M., López, R., Páez, E., Hernández, E., Reyes, M., Calcines, A., et al. 2012, *Astron. Nachr.*, 333, 872
- Couvidat, S., Schou, J., Shine, R. A., Bush, R. I., Miles, J. W., Scherrer, P. H., & Rairden, R. L. 2012, *Solar Phys.*, 275, 285
- Denker, C., Balthasar, H., Hofmann, A., Bello González, N., & Volkmer, R. 2010, in *Ground-Based and Airborne Instrumentation for Astronomy III*, edited by I. S. McLean, S. K. Ramsay, & H. Takami, vol. 7735 of *Proc. SPIE*, 77356M
- Denker, C., von der Lühe, O., Feller, A., Arlt, K., Balthasar, H., Bauer, S.-M., et al. 2012, *Astron. Nachr.*, 333, 810
- Hagenaar, H. J., & Shine, R. A. 2005, *ApJ*, 635, 659
- Harvey, K., & Harvey, J. 1973, *Solar Phys.*, 28, 61
- Kubo, M., Lites, B. W., Shimizu, T., & Ichimoto, K. 2008, *ApJ*, 686, 1447
- Leka, K. D., & Skumanich, A. 1998, *ApJ*, 507, 454
- Martínez Pillet, V. 2002, *Astron. Nachr.*, 323, 342
- Petrovay, K., & van Driel-Gesztelyi, L. 1997, *Solar Phys.*, 176, 249
- Puschmann, K. G., Denker, C., Kneer, F., Al Erdogan, N., Balthasar, H., Bauer, S. M., et al. 2012, *Astron. Nachr.*, 333, 880
- Rempel, M., & Cheung, M. C. M. 2014, *ApJ*, 785, 90
- Scherrer, P. H., Schou, J., Bush, R. I., Kosovichev, A. G., Bogart, R. S., Hoeksema, J. T., et al. 2012, *Solar Phys.*, 275, 207
- Schlichenmaier, R., Rezaei, R., Bello González, N., & Waldmann, T. A. 2010, *A&A*, 512, L1
- Schmidt, W., von der Lühe, O., Volkmer, R., Denker, C., Solanki, S. K., Balthasar, H., et al. 2012, *Astron. Nachr.*, 333, 796

- Schou, J., Scherrer, P. H., Bush, R. I., Wachter, R., Couvidat, S., Rabello-Soares, M. C., et al. 2012, *Solar Phys.*, 275, 229
- Schuck, P. W. 2005, *ApJ*, 632, L53
- 2006, *ApJ*, 646, 1358
- Verma, M., Balthasar, H., Deng, N., Liu, C., Shimizu, T., Wang, H., & Denker, C. 2012, *A&A*, 538, A109
- Verma, M., & Denker, C. 2011, *A&A*, 529, A153
- Wachter, R., Schou, J., Rabello-Soares, M. C., Miles, J. W., Duvall, T. L., & Bush, R. I. 2012, *Solar Phys.*, 275, 261
- Wöger, F., von der Lühe, O., & Reardon, K. 2008, *A&A*, 488, 375
- Wöger, F., & von der Lühe, O., II 2008, in *Advanced Software and Control for Astronomy II*, edited by A. Bridger, & N. M. Radziwill, vol. 7019 of *Proc. SPIE*, 70191E
- Yang, G., Xu, Y., Wang, H., & Denker, C. 2003, *ApJ*, 597, 1190